The Astrophysical Journal, 933:146 (7pp), 2022 July 10 https://doi.org/10.3847/1538-4357/ac7446

Extragalactic Magnetic Fields and the Arrival Direction of Ultra-high-energy Cosmic Rays

Cainã de Oliveira and Vitor de Souza
Instituto de Física de São Carlos, Universidade de São Paulo, Av. Trabalhador São-carlense 400, São Carlos, Brasil; caina.oliveira@usp.br, vitor@ifsc.usp.br
Received 2022 April 1; revised 2022 May 23; accepted 2022 May 24; published 2022 July 11

Abstract

We studied the propagation of ultra-high-energy cosmic rays in extragalactic magnetic fields (EGMFs). We report on the effect of the EGMF on the large-scale anisotropy signal measured at Earth. We show how a spurious dipolar and quadrupolar signal can be generated by the EGMF even if the source distribution is isotropic.

Unified Astronomy Thesaurus concepts: Ultra-high-energy cosmic radiation (1733); Extragalactic magnetic fields (507); Cosmic ray astronomy (324); Cosmic ray sources (328); Cosmic rays (329)

Supporting material: animation

1. Introduction

Ultra-high-energy cosmic rays (UHECR—charged particles—$E > 10^{18}$ eV) were first measured in the 1960s (Linsley 1963), and have been studied by several observatories (Nagano & Watson 2000; Abu-Zayyad et al. 2012; The Pierre Auger Collaboration 2015), and will be explored by new experiments (Martello 2017; Abbasi et al. 2021; Fenu et al. 2021; Kotera 2021; Olinto & Krizmanic 2021) in the next decades. Since 1966 (Greisen 1966; Zatsepin & Kuz'min 1966), it has been known that the sources of UHECR are relatively nearby (<hundreds of Mpc from Earth). Source candidates are scarce and only from a few classes of objects (Hillas 1984). Hypothetical weak ($\sim$ nG) and non-structured ($\sim$ Mpc correlation length) extragalactic magnetic fields were shown to cause small dispersion ($\sim$ degree) of the UHECR with low charges (proton) from the direction of their sources (Stanev et al. 2000). These arguments together led to the announcement of the rise of UHECR astronomy (Cronin 1999). However, even after a large number of events have been collected using the Pierre Auger Observatory (215030 with $E > 2.5$ EeV; Deligny 2019) and the Telescope Array (2287 with $E > 2.5$ EeV; Abbasi et al. 2016), the two main experiments in operation, the fundamental question remains unanswered: Where do they come from?

In this article, we discuss the main reason why this question was not yet answered. We show the extragalactic magnetic field (EGMF) can have structure and intensity strong enough to generate anisotropies of an originally isotropic distribution of sources. Previous studies (Lee et al. 1995; Tanco 1998; Dolag et al. 2005) have shown that a structured EGMF could not be ignored when interpreting UHECR arrival directions. The EGMF intensity has been measured by several techniques, including gamma-ray energy spectrum modulations of distant sources, Faraday rotation of the polarized radio emission from distant sources, and properties of the cosmic microwave background radiation (Subramanian 2016). However, very little can be inferred about the EGMF topology from these data because they are integrated measurements along the line of sight, which depends mainly on the perpendicular component of the field.

In the last years, the use of cosmological simulation constrained by the most updated measurements has led to sophisticated hypotheses about the structure of the EGMF (Neronov & Vovk 2010; Pshirkov et al. 2016; Subramanian 2016; Brown et al. 2017; Vazza et al. 2017). Recent works (Hackstein et al. 2016; Alves Batista et al. 2017; Wittkowski & Kampert 2018) have used structured EGMF models together with detailed source and propagation models to search for the best fit of the arrival directions data. In these studies, source distribution, composition, EGMF structure, photon background models, and high-energy interaction models are assumed to improve the description of the data making it very hard, on the other hand, to isolate the effect of each assumption. We focus on understanding only how the EGMF affects the determination of the source distribution based on the arrival directions of UHECR. We show for the first time that the EGMF can imprint its structure in the arrival direction distribution of UHECR even if the original flux leaving the sources is isotropic.

2. Anisotropic Arrival Directions

We evaluate the anisotropy profile of an ensemble of UHECR moving in three models of EGMF named: Cellular, Astrophysical, and Primordial. The models Astrophysical and Primordial[1] are realistic structured EGMF calculated with sophisticated magnetohydrodynamical simulations in a λCDM universe (Hackstein et al. 2018). The main difference between the Primordial and Astrophysical models is the seed field intensity of 0.1 nG and 10^{-11} nG at $z = 60$, respectively. In the Astrophysical model the magnetic field is generated by impulsive thermal and magnetic feedback in halos. Magnetohydrodynamical simulations evolve the seed field until the present time, taking several measured constraints into consideration. The Cellular model is a commonplace EGMF model characterized by domains with 0.37 Mpc size in which the field has random orientation and intensity given by a Kolmogorov spectrum with rms intensity of 3 nG. Most of the arrival directions studies of UHECR are based on the Cellular EGMF model (Lemoine et al. 1997; Stanev et al. 2000; Harari et al. 2002; Globus et al. 2019; Lang et al. 2020, 2021; Ding et al. 2021). We chose extreme models of EGMF to cover the entire range of possibilities.

[1] Models used here are named AstrophysicalR and Primordial in the reference Hackstein et al. (2018).

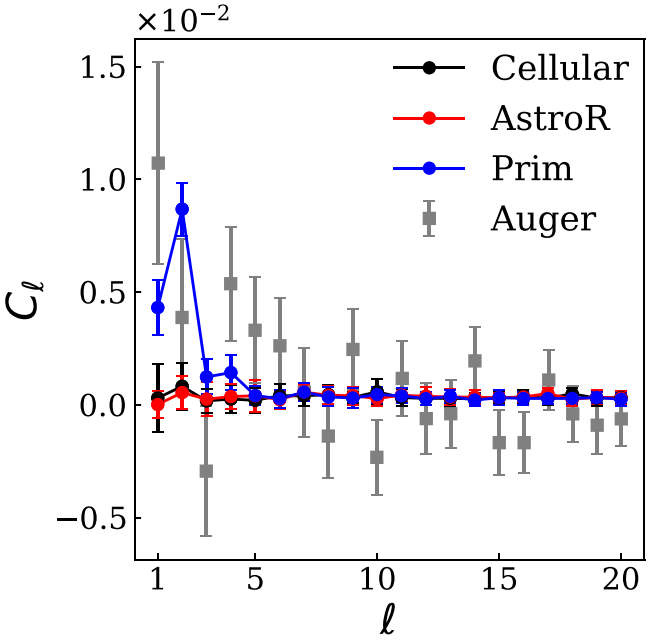

Figure 1. Angular power spectrum of the arrival directions of particles at Earth. Black, red, and blue dots show the result of the simulation of protons with energy between 32 and 1000 EeV following a power-law spectrum with spectral index −1, leaving 10^{10} sources distributed isotropically and uniformly up to 100 Mpc from Earth and traveling through Cellular, Astrophysical, and Primordial EGMF models, respectively. Gray squares show the measurement done by the Pierre Auger Collaboration (de Almeida 2021). The error bars of the simulation were calculated with the same number of events detected by the Pierre Auger Observatory.

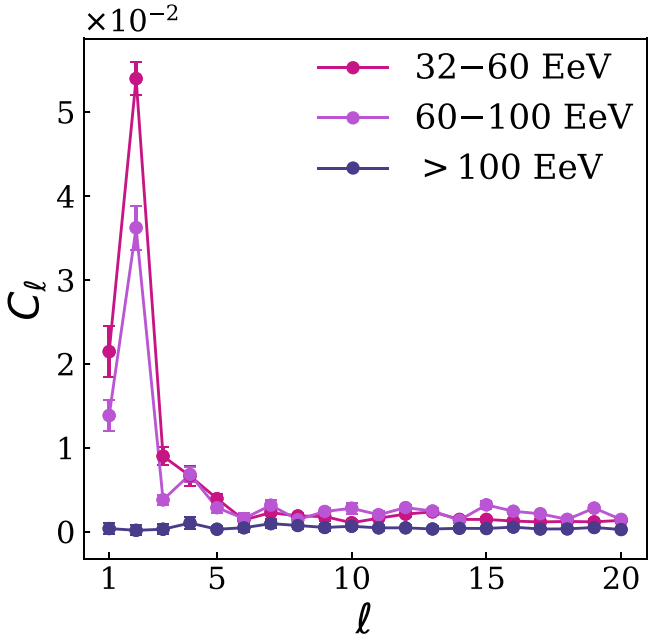

Figure 2. Angular power spectrum of the arrival directions of particles at Earth. The curves show the results of the simulation of protons following a power-law energy spectrum with spectral index −1, leaving 10^{10} sources distributed isotropically and uniformly up to 100 Mpc from Earth and traveling through the Primordial EGMF model until an observer with size 250 kpc was reached. Each curve represents the result for the subset of events in the energy ranges 32–60 EeV (red), 60–100 EeV (purple), and above 100 EeV (blue). The error bars of the simulation were calculated with the same number of events detected by the Pierre Auger Observatory (de Almeida 2021).

Using the software CRPropa 3 (Batista et al. 2016), we simulated 10^{10} protons leaving the sources and propagating in the three EGMF models described above. Sources are considered steady and isotropic emitters of UHECRs. The particles are followed until they travel a distance of 4 Gpc (the horizon to Hubble energy loss) well beyond the 100 Mpc scales involved in the simulations. The number of protons arriving on the observer sphere varies for each EGMF model. The results presented here used more than 40,000 detected events in each case. We use the uniform injection module to distribute the sources isotropically and uniformly up to 100 Mpc from Earth. Protons were simulated, leaving the sources with momentum randomly oriented and energy between 32 and 1000 EeV following a power-law spectrum with spectral index −1. This is the energy range of the data published by the Pierre Auger Collaboration in reference de Almeida (2021). The Cash–Karp (Cash & Karp 1990) integration algorithm was chosen to solve the Lorentz equation and the particles were propagated until they reached the surface of a sphere of radius 250 kpc centered at the Milky Way position. This observer size is significantly smaller and therefore more accurate than the typical values used in the literature. In Appendix we show that the conclusions presented here are independent of the integration algorithm and of the observer size. No other interaction besides the deflection in the extragalactic magnetic field was taken into account. In this way, the uncertainties concerning the radiation backgrounds and high-energy interactions are not influencing the calculation. The consequences of this simplification are discussed in Section 4. The Galactic magnetic field was considered according to the JF12 (Jansson & Farrar 2012) model.

Figure 1 shows the angular power spectrum of the arrival directions evaluated from the coefficients of the multipolar expansion ($C_\ell = \sum_{m=-\ell}^{\ell} |a_{\ell m}|^2/(2\ell+1)$) as a function of the spherical harmonic order (ℓ), as calculated with HealPix[2] (Gorski et al. 2005; Zonca et al. 2019). The angular power spectrum measured by the Pierre Auger Observatory for energies above 32 EeV (de Almeida 2021) is also shown. The same number of events measured by the Pierre Auger Observatory was used to calculate the error bars of the simulation. The Primordial EGMF model generates a large dipolar and quadrupolar component, while the Astrophysical model does not generate any significative anisotropy, with a signal compatible with that of the Cellular field. The spectrum is highly dependent on the EGMF model, which means the angular power spectrum can be used to determine the true EGMF if a realistic simulation of the sources is used in the interpretation of the data. This is not the case in the simulations presented here, in which we had the purpose of proving the EGMF effect on the generation of an anisotropic signal. Note that the number of events measured by the Pierre Auger Observatory leads to smaller error bars than the difference between the Primordial and the Astrophysical EGMF models. Figure 2 shows, as expected, that the anisotropy signal generated by the Primordial EGMF model vanishes with the increasing energy of the events.

Figure 3 shows the sky map in which the simulated flux of particles is shown for the Primordial EGMF with a Gaussian smoothing with full width at half maximum equal to 10°. Although the source is isotropically distributed, the anisotropy

[2] http://healpix.sourceforge.net

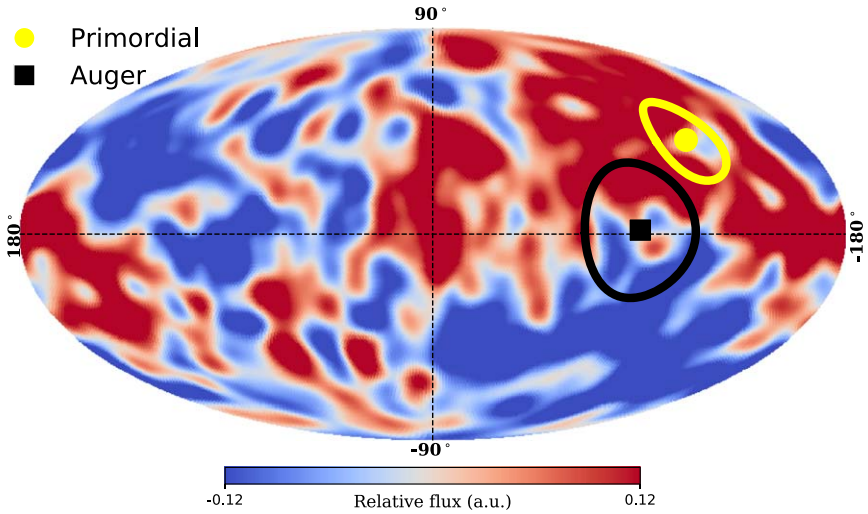

Figure 3. Map in Galactic coordinates and Aitoff projection of the arrival direction flux for the Primordial EGMF model when isotropic sources were simulated. A Gaussian smoothing with FWHM equal to 10° was used to highlight the anisotropy. The dipole direction of the simulation is shown in yellow and the dipole direction measured by the Pierre Auger Observatory (de Almeida 2021) is shown in black. The circular lines show the 68% C.L. on the direction reconstruction. The C.L. of the simulation was calculated with the same number of events detected by the Pierre Auger Observatory (de Almeida 2021). The complete simulation setup is identical to the one used in Figure 1.

in the arrival direction is clearly seen in the sky map. The direction of the dipoles generated by the Primordial EGMF and measured by the Pierre Auger Observatory is also shown (points and circles). The direction of the dipole generated by the Primordial EGMF is ($l = 236°$, $b = 34°$). A component of the measured dipole could be generated by a structured EGMF similar to the Primordial model instead of the source distribution. The Astrophysical EGMF model generates a negligible dipolar component. The differences between the Primordial and Astrophysical EGMF effects on the angular power spectrum can be understood based on the scale of the irregularities of each field.

3. Magnetic Field Topology and Scattering

The potential of a magnetic field to generate anisotropic arrival directions from an original isotropic flux depends on the field topology. Magnetic fields with abrupt changes in space or time scatter particles in collision-like interactions. The scattering process generates anisotropy and its efficiency depends on the magnitude of the magnetic irregularities as a function of the physical scale. Parseval's theorem allows the comparison of the physical and irregularities scales of the problem (Jokipii 1973; Longair 2011)

$$\int_{-\infty}^{\infty} B^2(k)dk = \int_{-\infty}^{\infty} B^2(r)dr \qquad (1)$$

where $B(k)$ is the Fourier transform of the magnetic field intensity in space, $B(r)$. The power density spectrum ($kB(k)\bar{B}(k)$) gives the energy in each Fourier component, revealing the scales in which the magnetic irregularities are more important. If the gyroradii of particles are larger than the important scale in the power density spectrum, the scattering is irrelevant and therefore any isotropic flux remains isotropic after interaction with the field.

Figure 4 shows the power density spectrum (black lines) of the Cellular, Astrophysical, and Primordial EGMF models in comparison to the gyroradius of 60 EeV protons (gray region). The calculation was done along perpendicular directions $r = x$, y, z in supergalactic coordinates. When traveling in the Cellular and Astrophysical EGMF (first and second columns of Figure 4), particles have gyroradii much larger than the scales important in the power density spectrum, therefore the fluctuations in the magnetic field cause only small changes in pitch angle, and the generation of anisotropies is not efficient. The important scales in the power density spectrum of the Primordial EGMF model (third column) are in wavelengths, $\lambda = 2\pi/k$, of the same size as these particles' gyroradii, therefore changes in pitch angle are large and the production of anisotropies is very efficient.

The match between the gyroradii for particles traveling in the Primordial EGMF and the scales of fluctuations of the field, explains why the Primordial EGMF is much more efficient than the Astrophysical EGMF in generating anisotropies.

4. Conclusions

In this article, we have shown that some structured EGMF models may generate anisotropies in the arrival directions of UHECR originally ejected by isotropically distributed sources. The amplitude of the dipole generated by the Primordial EGMF model used here is similar to the dipole measured by the Pierre Auger Observatory (see Figure 1). We show in Figure 3 that the dipole generated by the EGMF points 45°.2 away from the direction of the dipole measured by the Pierre Auger Collaboration. The measured dipole could have a contribution generated by the EGMF. Further considerations and limitations of the calculations presented here are discussed below.

The results presented here have several other consequences and interpretations. UHECR astronomy might be limited to nearby sources in specific directions. Our Galaxy is surrounded by magnetic walls deflecting UHECR away with collision-like interactions. The size of the magnetic horizon varies significantly with the direction (Hackstein et al. 2016). The flux at Earth from sources located in the interior of galactic clusters,

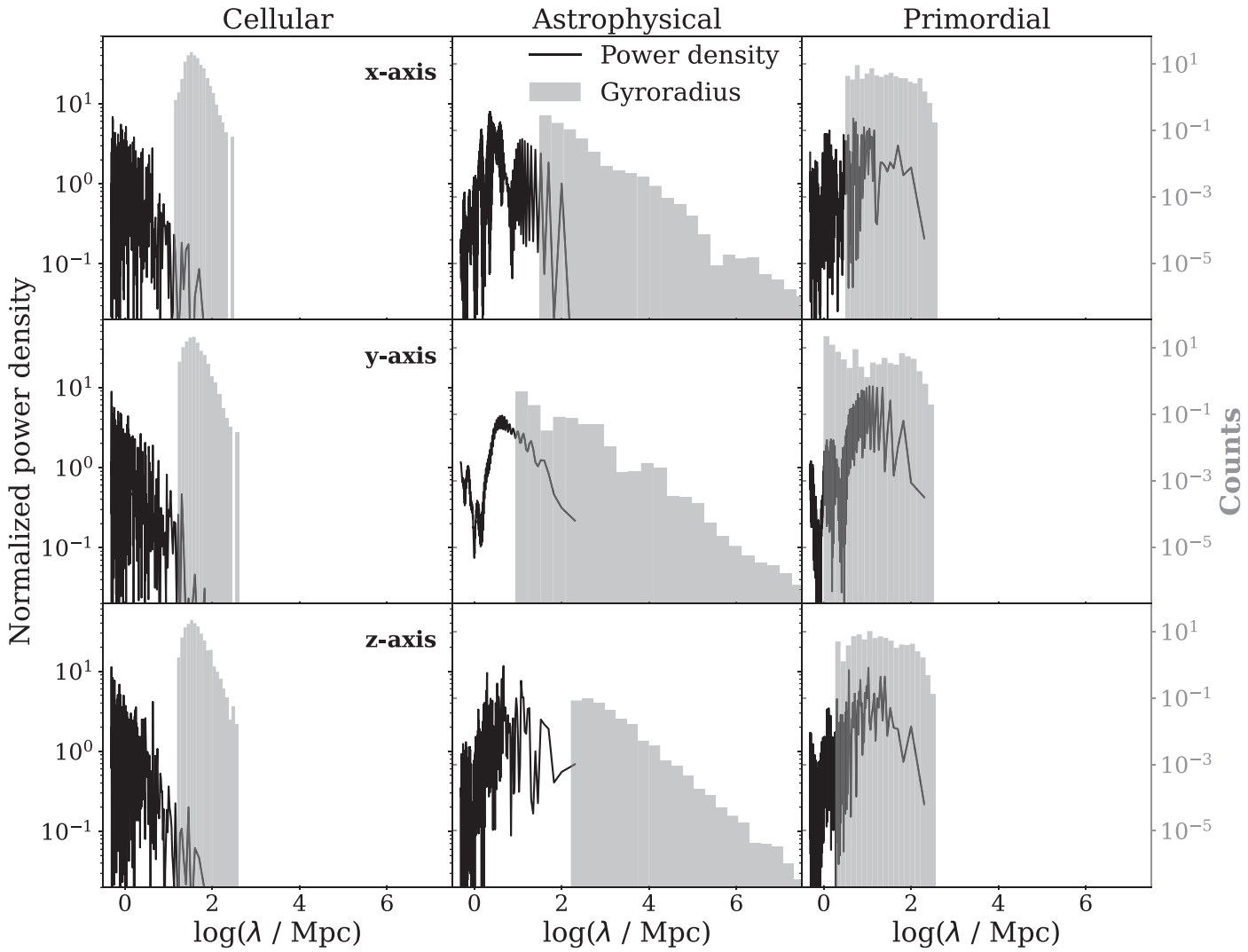

Figure 4. The normalized power density of the Cellular, Astrophysical, and Primordial EGMF models shown by black lines with values given by the left-hand side axis. Distribution of 60 EeV proton gyroradii in the corresponding EGMF models shown by gray bars with values given by the right-hand side axis. The calculation was done along perpendicular directions (x,y,z) in supergalactic coordinates.

for instance, Virgo A, is highly suppressed by the EGMF (Tanco 1998; de Oliveira & de Souza 2022). The angular power spectrum of the UHECR arrival direction is EGMF-dependent. Therefore, it is possible to discriminate among different EGMF models by measuring the angular power spectrum.

The interpretation of the measured arrival directions distribution of UHECR, including large-scale anisotropies analyzed with the angular power spectrum, must consider structured EGMF at least as systematic uncertainty. Each EGMF model generates a different arrival direction pattern correlated to the distribution and size of the field discontinuities. The Cellular model implies smooth propagation of UHECR, therefore no anisotropy is generated. The Astrophysical model has bubble-like discontinuities, not very different from a cellular-type EGMF field, therefore, no anisotropy is generated. The Primordial model has filament-like discontinuities trapping particles and generating strong anisotropies. This can be seen by the large quadrupolar signal generated by the Primordial model; as previously discussed (The Pierre Auger Collaboration 2014), a quadrupole signal can be caused by magnetic sheets following the distribution of mass in the supergalactic plane.

According to the discussion in Harari et al. (1999), the anisotropy generated by the Primordial model from originally isotropic distributions is compatible with the primary interpretation of Liouville's theorem. The highly magnetized structures trap particles and screen the detector from sources at given directions. This can be seen in the animated Figure in the online version of this paper, in which the evolution in time of the ensemble of particles in phase space is shown (Figure 5). Note the particles trapped in the EGMF make abrupt changes in the momentum. Further discussion about the validity of Liouville's theorem in a galactic and solar magnetic field can be found in López-Barquero et al. (2016, 2017); Ahlers & Mertsch (2017).

The quantitative results presented here are lower limits. Particles with larger charges, i.e., iron nuclei, have much larger deflections than the ones shown above for protons. The path length of nuclei also increases when fragmentation and energy-loss effects are considered on the way from the source to Earth, magnifying the deflections caused by the EGMF. A more negative value for the spectral index at the source would inject

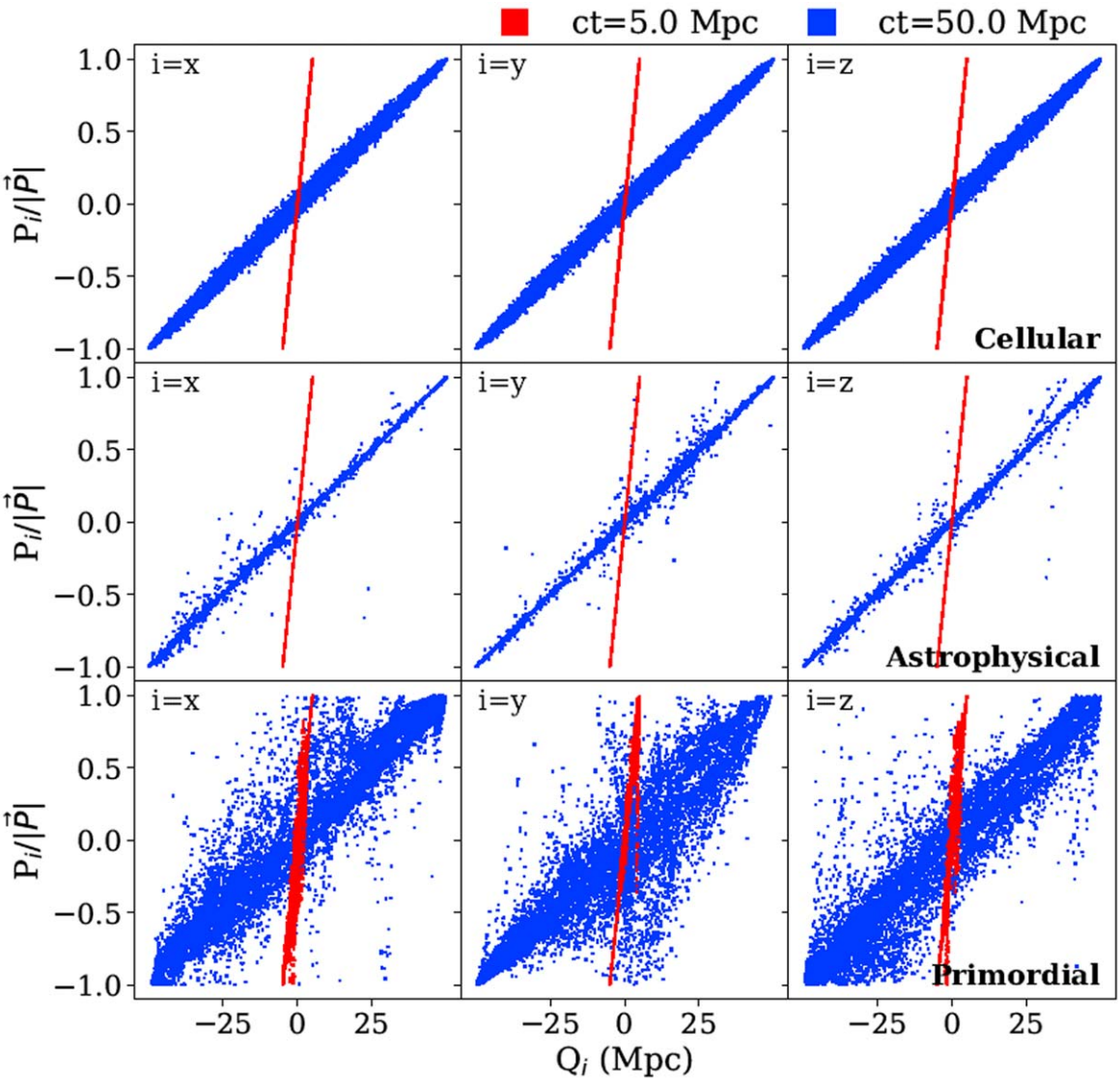

Figure 5. Generalized coordinate phase space of momentum P_i and position Q_i with $i = x, y, z$ in each panel. 10^4 simulated protons with energy 60 EeV leaving Earth with random directions are shown. Each point represents one particle. Two instants are shown: $ct = 5$ Mpc (red) and $ct = 50$ Mpc (blue). An animated version of this figure is available on the online version of this article. The animation begins at $ct = 0.5$ Mpc and ends at $ct = 50.0$ Mpc. The real-time duration of the animation is 14 s.
(An animation of this figure is available.)

a larger proportion of low energetic particles, which are easier to trap by the EGMF, also increasing the effect of the EGMF on the arrival direction distribution. The same conclusion is valid if the energy spectrum at the source has a cutoff. Despite more realistic simulations being important to analyze the data, they would only increase the strength of the conclusions reached here.

Authors thanks Leonardo Paulo Maia, Rogério Menezes, and Rodrigo Lang for useful discussions. C.O. and V.d.S. acknowledge FAPESP Projects 2021/01089-1, 2020/15453-4, and 2019/10151-2. The authors acknowledge the National Laboratory for Scientific Computing (LNCC/MCTI, Brazil) for providing HPC resources of the SDumont supercomputer (http://sdumont.lncc.br). V.d.S. acknowledges CNPq. This study was financed in part by the Coordenação de Aperfeiçoamento de Pessoal de Nível Superior—Brasil (CAPES) - Finance Code 001. Some of the results in this paper have been derived using the healpy and HEALPix package.

Appendix A
Study of the Simulation Parameters

We tested the dependence of the results presented in the paper in respect of: (a) integration algorithm, (b) observer size, and (c) influence of the galactic magnetic field. These aspects are known to have a strong influence on some anisotropic studies. Despite that, as shown in the next subsections, they do not interfere with the conclusions of this paper.

In the following studies, the number of events detected was above 40,000. For comparison, the error bars correspond to the sample standard deviation of the same number of events measured by the Pierre Auger Observatory (de Almeida 2021). All results in the Appendix are for the Primordial EGMF model for which the anisotropy signal was obtained.

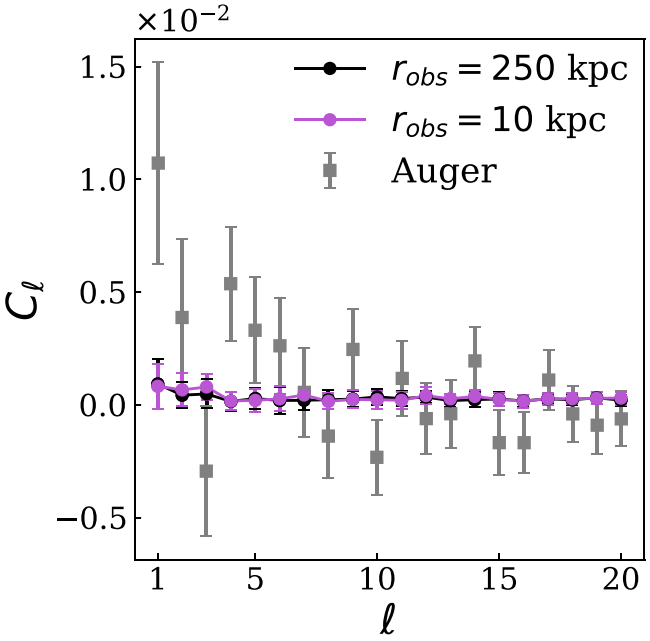

Figure 6. Angular power spectrum of the arrival directions of particles at Earth. Black and purple dots show the result of the simulation of protons with energy between 32 and 1000 EeV following a power-law spectrum with spectral index −1, leaving 6×10^6 (black) and 10^{11} (purple) sources distributed isotropically and uniformly up to 25 Mpc from Earth and traveling through the Primordial EGMF model. The observer size was 250 and 10 kpc for the black and purple dots, respectively. Gray squares show the measurement done by the Pierre Auger Collaboration (de Almeida 2021). The error bars of the simulation were calculated with the same number of events detected by the Pierre Auger Observatory.

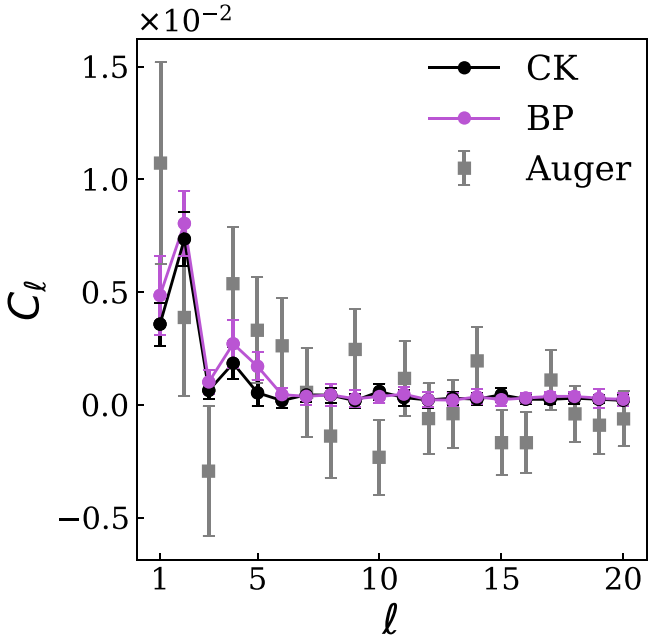

Figure 7. Angular power spectrum of the arrival directions of particles at Earth. Black and purple dots show the result of the simulation of protons with energy between 32 and 1000 EeV following a power-law spectrum with spectral index −1, leaving 10^{10} sources distributed isotropically and uniformly up to 100 Mpc from Earth and traveling through the Primordial EGMF model. Black and purple dots show the results for Cash–Karp (CK) and Boris push (BP) integration algorithms. The observer size was 250 kpc. Gray squares show the measurement done by the Pierre Auger Collaboration (de Almeida 2021). The error bars of the simulation were calculated with the same number of events detected by the Pierre Auger Observatory.

A.1. Effect of the Observer Radius

The effect of the observer size was checked, changing the observer radius ($r_{\rm obs}$) from 250 to 10 kpc. Sources were uniformly distributed within 25 Mpc from Earth. A smaller observer radius significantly increases the computational cost of the simulations. In order to have more than 40,000 particles detected, we needed to inject 6×10^6 and $\sim 10^{11}$ particles for $r_{\rm obs} = 250$ kpc and $r_{\rm obs} = 10$ kpc, respectively.

The angular power spectra in Figure 6 show that the uncertainty related to the observer size is negligible, since the differences are much smaller than the statistical fluctuations.

A.2. Effect of the Integration Method

We tested the effect of the integration algorithm in the conclusions presented in the paper (Section 4) by comparing the results using the Cash–Karp (CK) and Boris push (BP; Boris & Naval Research Laboratory 1971) algorithms, both implemented in CRPropa 3. In this test, sources were uniformly distributed within 100 Mpc from Earth.

The main difference between both methods, in respect of particle propagation in the magnetic field, is how energy conservation is implemented. The BP algorithm has energy conservation implemented by construction while CK does not. When CK is used, CRPropa must force energy conservation in each step. A large comparison between both methods is presented in reference (The CRPropa Developers 2022)

The angular power spectra in Figure 7 show that the uncertainty related to the integration methods is negligible, since the differences are much smaller than the statistical fluctuations.

A.3. Effect of the Galactic Magnetic Field

We tested the effect of the galactic magnetic field in the conclusions presented in the paper by comparing the results with and without the galactic magnetic field.

The angular power spectra in Figure 8 show that the uncertainty related to the galactic magnetic field is negligible since the differences are much smaller than the statistical fluctuations.

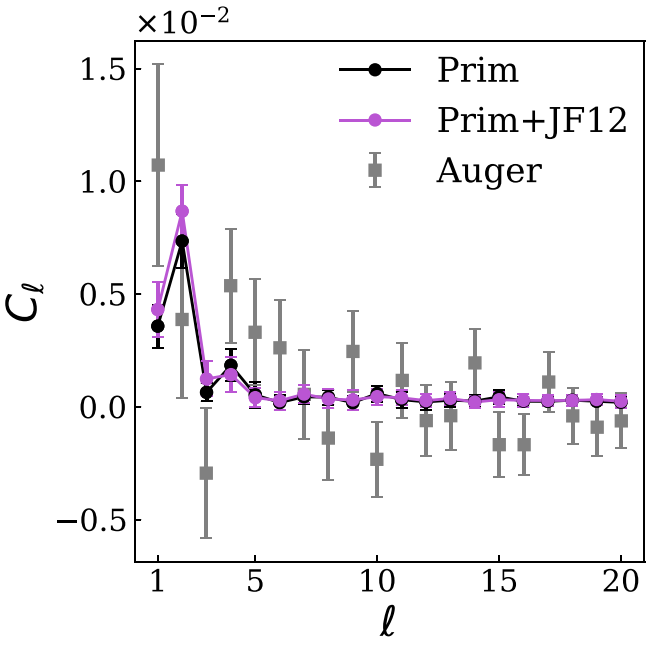

Figure 8. Angular power spectrum of the arrival directions of particles at Earth. Black and purple dots show the result of the simulation of protons with energy between 32 and 1000 EeV following a power-law spectrum with spectral index −1, leaving 10^{10} sources distributed isotropically and uniformly up to 100 Mpc from Earth and traveling through the Primordial EGMF model. Black and purple dots show the results when the JF12 galactic magnetic field was used (purple) and not used (black). The observer size was 250 kpc. Gray squares show the measurement done by the Pierre Auger Collaboration (de Almeida 2021). The error bars of the simulation were calculated with the same number of events detected by the Pierre Auger Observatory.

ORCID iDs

Cainã de Oliveira https://orcid.org/0000-0003-4038-1509
Vitor de Souza https://orcid.org/0000-0003-0865-233X

References

Abbasi, R., Abu-Zayyad, T., Allen, M., et al. 2021, in 37th Int. Cosmic Ray Conf. (ICRC2021), Vol. 395 (Trieste: SISSA), 393
Abbasi, R. U., Abe, M., Abu-Zayyad, T., et al. 2016, APh, 80, 131
Abu-Zayyad, T., Aida, R., Allen, M., et al. 2012, NIMPA, 689, 87
Ahlers, M., & Mertsch, P. 2017, PrPNP, 94, 184
Alves Batista, R., Shin, M.-S., Devriendt, J., Semikoz, D., & Sigl, G. 2017, PhRvD, 96, 023010
Batista, R. A., Dundovic, A., Erdmann, M., et al. 2016, JCAP, 2016, 038
Boris, J. & Naval Research Laboratory 1971, in Proc. Conf. Numerical Simulation of Plasmas, Vol. 4 (Washington, DC: The Naval Research Laboratory), 3, https://apps.dtic.mil/sti/pdfs/ADA023511.pdf
Brown, S., Vernstrom, T., Carretti, E., et al. 2017, MNRAS, 468, 4246
Cash, J. R., & Karp, A. H. 1990, ACM Trans. Math. Softw., 16, 201
Cronin, J. W. 1999, RvMP, 71, S165
de Almeida, R. 2021, in Proc. 37th Int. Cosmic Ray Conf. (ICRC2021), Vol. 395 (Trieste: SISSA), 335
de Oliveira, C., & de Souza, V. 2022, ApJ, 925, 42
Deligny, O. 2019, in 36th Int. Cosmic Ray Conf. (ICRC2019), Vol. 358 (Trieste: SISSA)
Ding, C., Globus, N., & Farrar, G. R. 2021, ApJL, 913, L13
Dolag, K., Grasso, D., Springel, V., & Tkachev, I. 2005, JCAP, 2005, 009
Fenu, F., Sharakin, S., Zotov, M., et al. 2021, in 37th Int. Cosmic Ray Conf. (ICRC2021), Vol. 395 (Trieste: SISSA), 409
Globus, N., Piran, T., Hoffman, Y., Carlesi, E., & Pomarède, D. 2019, MNRAS, 484, 4167
Gorski, K. M., Hivon, E., Banday, A. J., et al. 2005, ApJ, 622, 759
Greisen, K. 1966, PhRvL, 16, 748
Hackstein, S., Vazza, F., Brüggen, M., Sigl, G., & Dundovic, A. 2016, MNRAS, 462, 3660
Hackstein, S., Vazza, F., Brüggen, M., Sorce, J. G., & Gottlöber, S. 2018, MNRAS, 475, 2519
Harari, D., Mollerach, S., & Roulet, E. 1999, JHEP, 1999, 022
Harari, D., Mollerach, S., & Roulet, E. 2002, JHEP, 2002, 006
Hillas, A. M. 1984, ARA&A, 22, 425
Jansson, R., & Farrar, G. R. 2012, ApJ, 757, 14
Jokipii, J. R. 1973, ARA&A, 11, 1
Kotera, K. 2021, in 37th Int. Cosmic Ray Conf. (ICRC2021), Vol. 395 (Trieste: SISSA), 1181
Lang, R. G., Taylor, A. M., Ahlers, M., & de Souza, V. 2020, PhRvD, 102, 063012
Lang, R. G., Taylor, A. M., & de Souza, V. 2021, PhRvD, 103, 063005
Lee, S., Olinto, A. V., & Sigl, G. 1995, ApJL, 455, L21
Lemoine, M., Sigl, G., Olinto, A. V., & Schramm, D. N. 1997, ApJ, 486, L115
Linsley, J. 1963, PhRvL, 10, 146
Longair, M. S. 2011, High Energy Astrophysics (3rd edn; Cambridge: Cambridge Univ. Press)
López-Barquero, V., Farber, R., Xu, S., Desiati, P., & Lazarian, A. 2016, ApJ, 830, 19
López-Barquero, V., Xu, S., Desiati, P., et al. 2017, ApJ, 842, 54
Martello, D. 2017, in 35th Int. Cosmic Ray Conf. (ICRC2017), Vol. 301 (Trieste: SISSA), 383
Nagano, M., & Watson, A. A. 2000, RvMP, 72, 689
Neronov, A., & Vovk, I. 2010, Sci, 328, 73
Olinto, A. V., & Krizmanic, J. 2021, in 37th Int. Cosmic Ray Conf. (ICRC2021), Vol. 395 (Trieste: SISSA), 976
Pshirkov, M. S., Tinyakov, P. G., & Urban, F. R. 2016, PhRvL, 116, 191302
Stanev, T., Engel, R., Mücke, A., Protheroe, R. J., & Rachen, J. P. 2000, PhRvD, 62, 093005
Subramanian, K. 2016, RPPh, 79, 076901
Tanco, G. A. M. 1998, ApJ, 505, L79
The CRPropa Developers 2022, CRPropa 3—Webpage, https://crpropa.github.io/CRPropa3/pages/example_notebooks/propagation_comparison/Propagation_Comparison_CK_BP.html
The Pierre Auger Collaboration 2014, ApJ, 794, 172
The Pierre Auger Collaboration 2015, NIMPA, 798, 172
Vazza, F., Brüggen, M., Gheller, C., et al. 2017, CQGra, 34, 234001
Wittkowski, D., & Kampert, K.-H. 2018, ApJ, 854, L3
Zatsepin, G. T., & Kuz'min, V. A. 1966, ZhETF Pis'ma, 4, 114
Zonca, A., Singer, L., Lenz, D., et al. 2019, Journal of Open Source Software, 4, 1298